Usak University

Journal of Engineering Sciences

An international e-journal published by the University of Usak

Journal homepage: dergipark.gov.tr/uujes

Research article

CLASSIFICATION WITH MACHINE LEARNING METHODS FROM MULTI-SEQUENCE MR IMAGES OF CHILDHOOD POSTERIOR FOSSA TUMORS

Nuray Demiröz[1], Semra İçer[1], Zehra Filiz Karaman[2]*

[1]Department of Biomedical Engineering, Erciyes University, Türkiye
[2]Pediatric Radiology, Erciyes University, Türkiye

Received: June 24, 2024 Revised: December 2, 2024 Accepted: December 2, 2024 Online available: December 30, 2024

Abstract

Childhood brain tumors rank high among the leading causes of mortality, being the second most common type of cancer after leukemia. Abnormal structures in the brain are visualized using MRI techniques, which are the most employed tools for distinguishing the neural structure of the human brain. However, identifying and diagnosing these abnormal structures can be a time-consuming and critical process. In this study, tumors in the Magnetic Resonance images of patients with Posterior Fossa tumors were segmented using two different image segmentation methods. Subsequently, numerical features were extracted from these tumors, and significant numerical features among tumor groups were determined using the Student's T-test; based on these features, tumor types were classified using machine learning algorithms. The study focused on the three most common types of Posterior Fossa tumors: Medulloblastoma, Ependymoma, and Pilocytic Astrocytoma, utilizing T2, Contrast-Enhanced T1, and ADC sequences. A total of forty-eight different numerical features were extracted from the segmented tumors and then acquired significant features were classified using five different machine learning algorithms. Among PA-MB, EM-MB and EM-PA tumor types, the average result of the most successful method in the T1 sequence was 86.93%, while it was 93.7% for the T2 sequence and 92.06% for the ADC sequence. Decision tree, SVM and Ensemble classifiers gave more successful results than others. As a result of the detailed examination, our study not only makes valuable contributions to the literature, but also has a promising structure in terms of its potential to help clinicians.

Keywords: *Posterior Fossa tumors; Image Processing; Feature Extraction; Machine Learning.*

1. Introduction

Posterior fossa tumors are brain tumors that occur in the region known as the "posterior fossa," located at the lower back of the skull. They are among the malignancies that cause

*Corresponding author: Prof. Dr. Semra İÇER
E-mail: ksemra@erciyes.edu.tr

DOI: 10.47137/uujes.1501424

numerous fatalities in children. Also known as "infratentorial tumors," these tumors are predominantly benign tumors of the auditory and balance nerves, but in some cases, they can be malignant. Posterior fossa tumors are considered one of the most critical brain lesions. When they involve the brainstem within the posterior fossa, they become one of the most devastating forms of human diseases. Posterior fossa tumors account for 50-74% of childhood tumors, with pilocytic astrocytomas (PA), medulloblastomas (MB), ependymomas (EM), and brainstem gliomas being the most common types [1, 2]. Posterior fossa tumors have shown an increasing survival rate in recent years as a result of advances in treatment. However, since their prognoses and treatments vary due to the diversity in their molecular subtyping, early diagnosis and rapid and appropriate treatment are very important [3]. While these tumors may show similar characteristics among individuals in terms of age of onset and clinical symptoms, their clinical diagnosis can commonly be made by MRI. Conventional MRI is an extremely effective tool in detecting brain tumors and evaluating the location of the tumor and its effect on surrounding structures. However, since pediatric posterior fossa tumors have similar appearances, it has a limited role in the diagnosis of tumor type. Applications to increase the diagnostic accuracy of MRI using apparent diffusion coefficient (ADC) maps, MR spectroscopy, and MR perfusion are common. However, each of these applications is individually time-consuming, requires expertise, and is difficult to evaluate together [4,5]. Also, each tumor type can have variable appearances within the same group, and it is also expected that the diagnosis obtained from conventional radiological reporting may not always be entirely accurate. Accurately distinguishing and identifying posterior fossa tumors is a challenging and critically important process for healthcare professionals, as it plays a vital role in planning necessary and effective treatment to improve survival rates in patients. In this regard, the accuracy of diagnosis and treatment relies on the radiologist's education, expertise, and decision-making. For pediatric brain tumors, the accuracy of the diagnosis with MRI based on traditional radiological reporting is determined to be 63%, while the retrospective examination of images with expert review can increase the diagnostic accuracy up to 71% [6]. A precise and effective diagnostic process can aid in preoperative evaluation for patients with different tumor types and guide surgical planning. It serves as a guiding tool during surgical procedures. Image processing methods are extensively used in various fields in the healthcare domain, allowing meaningful numerical features to be extracted and analyzed from medical images. Machine learning [2] algorithms are widely utilized methods for finding relationships between data, making them suitable for tumor classification. In order to increase the survival rate of individuals by early and accurate diagnosis of Posterior Fossa tumors, utilizing image processing algorithms to identify significant numerical features in segmented tumors, and distinguishing tumors from each other using machine learning algorithms have been represents a potential method and it which can provide significant advantages beyond traditional approaches for diagnosis. Combining image processing and machine learning algorithms for tumor classification can provide support to radiology experts, facilitating accurate and early diagnosis, and streamlining clinical workflows. In the literature, numerous studies have examined posterior fossa tumors from various perspectives, including radiological and imaging features, pathological and histological characteristics, as well as distinguishing tumor subtypes and classifying tumors. Table 1 below gives a comparative table of publications similar to our study during the review of the literature. This table provides a clear overview of each study, highlighting the researchers, study focus, participant count, methods used, and the accuracy achieved. The shape and topography of posterior fossa tumors are similar, and since quantitative analysis is not routinely performed, it is difficult to select them radiologically or clinically with high accuracy and reliability. Obtaining quantitative features from images with many approaches as a result of image processing techniques that can be obtained from MR images creates a potential wealth of information that cannot be seen by the human eye [7,8]. The aim of our study is to enable the typing of these types of posterior fossa tumors seen in childhood using MRI images taken in different sequences. For this purpose, tumor segmentation was performed automatically before T2, contrast-enhanced T1

and ADC images of PA, MB, and EM tumors, and then many features were extracted for each sequence image and classified with machine learning methods.

Table 1 Examples from similar studies obtained as a result of literature research

Researchers	Focus	Participants	Methods	Accuracy
[9]Bidiwala and Pitmann (2004)	EM, MB, PA tumor classification	33 individuals	CT, MRI, Radiographic findings, Neural Network (not have image processing)	85.7%
[10]Gutiérrez et al.(2014)	EM, PA, MB tumor classification	40 children	Shape, histogram, texture features, SVM (T2, T1, ADC)	MB:95.8% EM:94.3% PA:96.9%
[11]Li et al. (2019)	EM, MB tumor analysis	174 patients	Machine learning, MR biomarkers	85.38%
[7]Zhou et al. (2020)	MB, EM, PA tumor classification	288 patients	Preoperative MR images, radiomic features, Tree-Based Pipeline Optimization Tool (T2, T1, ADC)	MB: 94%, EM: 84%, PA: 94%
[12]Zarinabad et al. (2018)	Metabolite analysis for tumor classification	41 pediatric patients	MR spectroscopy data, SVM, random forest, linear discriminant analysis (T2, T1)	MB: 86% EM: 90% PA: 90%
[8]Wang et al. (2022)	MB, PA, EM tumor analysis	99 patients	MRI-based analysis, high-dimensional features, random forest classifier (T2, T1, ADC)	93.81%
[13]Sotoudeh et al. (2023)	PA and HB tumor classification	34 PA, 18 HB patients	Post-contrast T1 sequence, various machine learning methods (T1)	82%
[14]Li et al. (2020)	Preoperative classification of EM and PA	45 patients	Radiomic analysis, machine learning algorithms, SVM	87.75%
[15]Quon et al. (2020)	Tumor detection and classification	92 children	Deep learning, modified ResNeXt-50-32x4d (T2-weighted MRI)	92%
[16]Fetit et al. (2018)	EM, MB, PA tumor classification	134 individuals	SVM, three-dimensional textural features from MRI	72%

When our study is compared with the sample studies in the literature given in Table 1, it can be seen that these studies either did not use automatic segmentation methods, manually segmented the tumor, or studied all of them in general without focusing on different types of posterior fossa tumors separately, or for each sequence used in clinical routine (it is seen that contrast-enhanced T1, T2, ADC) are not evaluated separately or there are differences in the extracted features and machine learning method. Additionally, it appears that these studies did not present each sequence and each tumor type in detail when presenting their results. Our study aims to extract and classify the image features of the three most common Posterior Fossa tumors in childhood: ependymoma (EM), medulloblastoma (MB), and pilocytic astrocytoma (PA). In the study, MR images obtained from T2, contrast-enhanced T1, and ADC sequences,

which are used separately or in combination for the clinical diagnosis of these tumors, were utilized. The tumor region in the images was segmented using the two most accurate segmentation methods, as verified by radiologists after trying the most commonly used segmentation methods in the literature. Subsequently, numerous numerical features were extracted from the images of each sequence. Unlike focusing on a single slice with the tumor, our study examined all slice where the tumor was visible. The numerical features that were meaningful for the images were determined using the Student's t-test from the extracted numerical features. This comprehensive analysis of the tumor from its inception to its conclusion in the images has increased the accuracy of the study. Among all the features obtained for each image (these; basic first-order statistical features, texture features based on the gray level co-occurrence matrix, features based on wavelet transform, numerical features based on percentages, and features from the histogram of oriented gradients (HOG)) those significant in discriminating between groups were identified. These identified features were then classified using five different machine learning algorithms, suitable for the study, to achieve high efficiency and accuracy in results. Our study holds promise in providing clinical support to radiologists by indicating which meaningful features each sequence possesses, which sequences and features better classify each tumor type, and also which classifier achieves higher success. As a result of the detailed examination, our study not only makes valuable contributions to the literature, but also has a promising structure in terms of its potential to help clinicians.

2. Methods

2.1 Patients and Image Dataset

This study was conducted using brain MR images of individuals aged between 0 and 18, diagnosed with Posterior Fossa tumors at the Department of Pediatric Radiology, Erciyes University. The images were obtained following the approval of the Erciyes University Clinical Research Ethics Committee. The study focused on the three most seen types of Posterior Fossa tumors: medulloblastoma, pilocytic astrocytoma, and ependymoma. The study was carried out on images of these tumor types in T2-weighted, contrast-enhanced T1-weighted, and ADC sequences. A small number of patients did not have images of all sequences. For patients with medulloblastoma, one individual lacked T1 sequence images, and two lacked ADC sequence images. For patients with ependymoma, two individuals lacked ADC sequence images, and five lacked T1 sequence images. Patients with pilocytic astrocytoma had complete sequence images. The images were acquired using the Siemens Magnetom Aera device on a 1.5T MR system with the same acquisition protocol. The acquired images consist of slices with a thickness of 5mm or 1mm, with a slice gap of 1mm. All images were acquired in DICOM format and are in grayscale. All sections containing tumors in any individual's images have been included in the study. Table 1 provides the number of patients and slices examined for three different sequences.

Table 2 Number of patients and slices examined for posterior fossa tumor

	T2 SEQUENCE / Number of Patients - Slices	**T1 SEQUENCE / Number of Patients - Slices**	**ADC SEQUENCE/ Number of Patients - Slices**
MEDULLOBLASTOMA	11 - 45	10 - 47	9 - 23
EPENDYMOMA	12 - 44	7 - 26	10 - 33
PILOCYTIC ASTROSITOMA	5 - 17	5 - 18	5 - 16
TOTAL	28 - 106	22 - 91	24 - 72

2.2 Image Processing and Segmentation

Image processing is a method that involves the acquisition, processing, analysis, and interpretation of visual information [17]. In this study, MRI images of patients diagnosed with Posterior Fossa were examined based on the number and thickness of slices for contrast-enhanced T1, T2, and ADC sequences. For subsequent analyses, all slices in which the tumor was visible in each sequence were determined and the slices containing the tumor were confirmed by the expert radiologist who is one of the authors of our study. In all images, the size was fixed at 730x730 pixels, ensuring that only the brain is included in the images. Subsequently, contrast-limited adaptive histogram equalization was applied to enhance image quality and eliminate color distortions. Tumor segmentation was attempted by taking all slices in which the tumor was visible from the images of all people in each sequence - an average of 5-6 sections from each person. In the literature, the most successful algorithms among the most commonly used image segmentation methods have been selected. The selection of the most successful segmentation algorithms was made in collaboration with the radiology expert in our research team, considering the success in each individual and slice. Tumors were extracted using two different algorithms: the Expectation Maximization algorithm and the Region-Based Active Contour algorithm. The selection of these two algorithms was primarily based on the advantages of Expectation Maximization, such as its wide application area, ability to handle missing data, capability to work with complex models, and applicability in clustering. Additionally, the Region-Based Active Contour algorithm was chosen for its resistance to noise in images, high accuracy in segmenting non-homogeneous areas, versatility in various applications, and its ability to precisely delineate the boundaries of objects. The process steps followed in the study are illustrated in the flowchart in Figure 1.

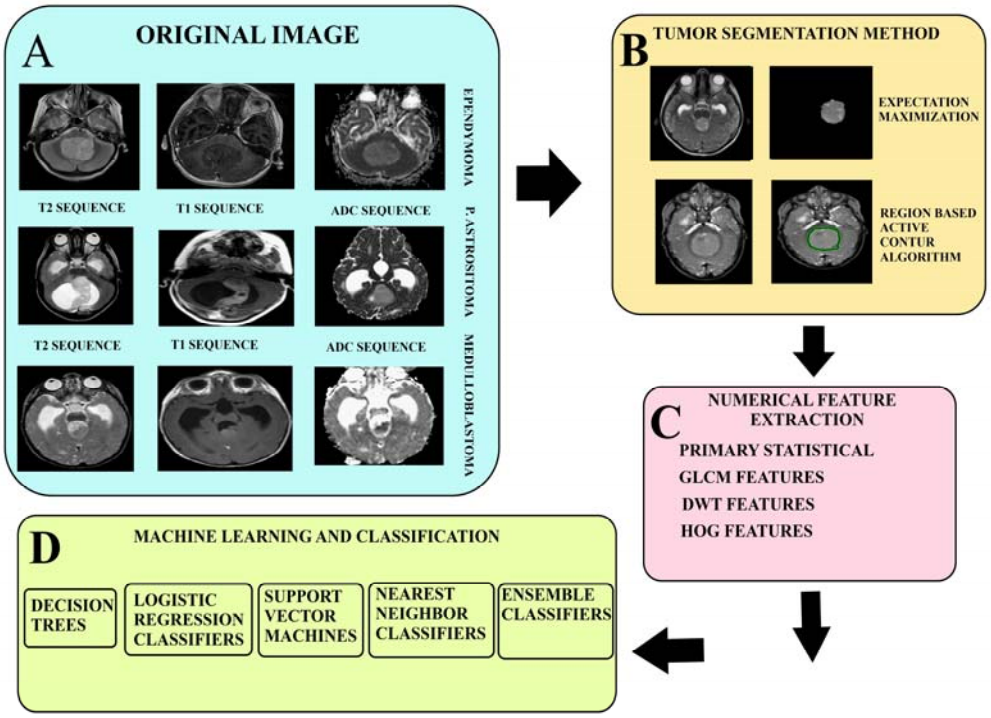

Fig. 1. Flow chart showing the steps followed in the research. Diagram A shows images of the tumor types and sequences studied. In diagram B, the methods used for segmentation and the tumors extraction with these methods are visualized. While numerical feature extraction methods are included in the C scheme, machine learning methods used in the D scheme are included.

2.2.1 Image segmentation with expectation maximization algorithm

The presence of the capability of the Expectation Maximization algorithm in medical image processing to calculate missing data in images has a significant impact on its inclusion in this study. It is an effective iterative process used to calculate the maximum likelihood when data is missing or hidden. In this iterative process, the procedure is repeated until reliable parameter estimates are obtained. The primary aim of maximum likelihood estimation is to estimate the model parameters that are most likely to generate the observed data. The EM algorithm consists of two steps in each iteration: the E-step and the M-step. In the E-step, also known as the expectation step, missing data is estimated when observed data and existing model parameters are provided. The term "expectation" is used because this process is performed using conditional expectations. In the M-step, the likelihood function is maximized under the assumption that missing data is known. The missing data estimates obtained from the E-step are used in place of the actual missing data. With each iteration, the likelihood increases, leading to convergence [18]. Below, Figure 2 contains sections belonging to the Medulloblastoma tumor type, and the tumor image extracted from these sections is presented using the Expectation Maximization algorithm.

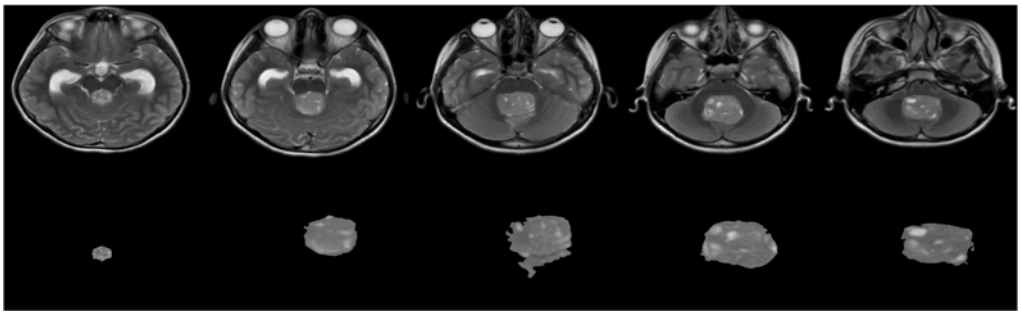

Fig. 2. Cross-sections specific to the Medulloblastoma tumor type extracted from this section using the Expectation Maximization algorithm, and the extracted tumor images.

2.2.2 Region-Based active contour algorithm for image segmentation

Region-based active contour segmentation in image processing locates the outer boundaries of the desired object in the image and estimates the object's region. This process involves automatically identifying boundaries on the image, starting from a pre-defined initial position. Determining the object's boundaries simplifies the segmentation process. This method significantly facilitates boundary delineation in images with noise or complex tonal variations. The Region-Based Active Contour algorithm is widely used in various fields and applications, such as visual tracking and image segmentation. The fundamental idea behind this algorithm is to deform a contour to produce the desired segmentation by minimizing a specific energy function. Active contours are composed of two main classes: edge-based and region-based active contour models [19]. In this study, the region-based active contour model is utilized. The region-based active contour model aims to channelize the movement of the active contour without using image gradients by defining relevant regions. This model provides better results in images with weak object boundaries [20]. In this study, region-based active contour segmentation was performed using Chan-Vese's edgeless active contour method [21]. This method is typically favored for images with homogeneity. It is a widely used approach in various fields, including medical image processing and object recognition. Both segmentation methods were implemented using Matlab. Below, Figure 3 displays cross-sectional images specific to the Ependymoma tumor type, along with the tumor region extracted from these sections using the region-based active contour algorithm.

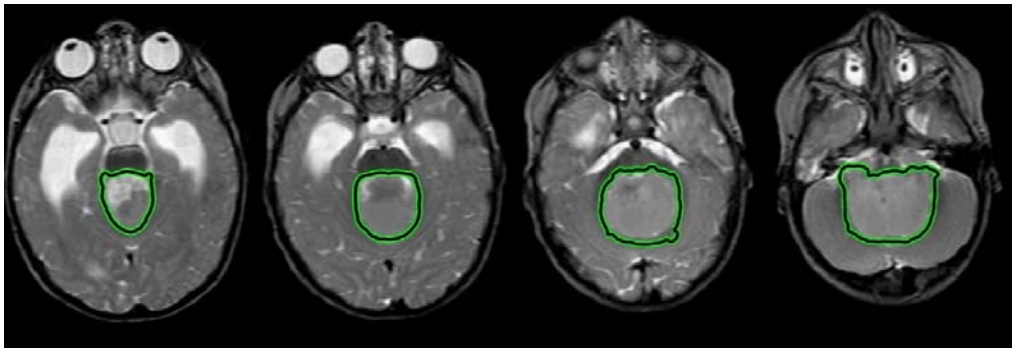

Fig. 3. The cross-sectional images belonging to the Ependymoma tumor type and the tumor images extracted from these sections are displayed. This extraction process was performed using the region-based active contour algorithm.

2.3 Numerical Feature Extraction

Images carry a significant amount of information that contributes to the overall meaning of the images. The purpose of extracting numerical features is to identify specific characteristics that uniquely distinguish images from one another. However, not all numerical features extracted from images are meaningful. In this study, numerical features were extracted using the Matlab program through five different methods. Initially, basic statistical features (such as minimum value, maximum value, entropy, etc.) provided 8 features. 22 features were identified from the Gray-Level Co-occurrence Matrix (GLCM), 8 features were obtained based on the Discrete Wavelet Transform (DWT), 8 features were derived from the Histogram of Oriented Gradients (HOG), and finally, 2 features were extracted from percentage values. These methods were used as they are known, run with default values, and applied to our data. In total, 48 features were obtained for all tumor types and imaging sequences. Numerical features that could provide discrimination for all tumor types were identified using the most used methods in the literature. Meaningful features for all sequences were determined using 4 different methods. The extracted numerical features were organized into a table, and significant features were determined using Student's t-Test in the Matlab program.

2.3.1 Primary Statistical Features

Primary statistical features are directly derived from the gray-level histogram of MRI images and encompass fundamental statistical characteristics inherent to the image. Within this investigation, a total of 8 primary statistical features were extracted, encompassing the minimum value, maximum value, mean value, standard deviation, variance, kurtosis, skewness, and entropy.

2.3.2 Second-Order Gray-Level Co-Occurrence Matrix (GLCM) Based Texture Features

The Gray-Level Co-occurrence Matrix (GLCM) is a statistical method that examines textures by reviewing the spatial relationships of pixels. It calculates how frequently pairs of pixels with a specific value and a specific contextual relationship occur in the image, characterizing the texture of the image. This matrix enables the computation of various statistical values [22].In medical image processing, in addition to features such as shape and size, texture features also hold great significance. By formulating second-order statistical features, features that define various tissues can be extracted. The GLCM matrix indicates how frequently different combinations of gray levels occur together in images [23]. In this study, a total of 22 second-order texture features were calculated using the GLCM. These features include:

Autocorrelation, Contrast, Correlation 1, Correlation 2, Cluster Prominence, Cluster Shade, Dissimilarity, Energy, Entropy, Homogeneity 1, Homogeneity 2, Maximum Probability, Sum of Squares, Sum Average, Sum Variance, Sum Entropy, Difference Variance, Difference Entropy, Information Measure of Correlation 1, Information Measure of Correlation 2, Normalized Inverse Difference and Inverse Difference Moment.

2.3.4 Discrete Wavelet Transform-Based Features

The Discrete Wavelet Transform (DWT) is a wavelet transform method that provides information about time and frequency content. DWT decomposes signals into different frequency bands, separating frequencies into various levels of resolution. It decomposes the image horizontally with low frequencies corresponding to vertical high frequencies, working with low-pass and high-pass filters. In the case of low-pass and high-pass filters, the former always provides convergence in the image, while the latter imparts edge information in the image [24]. Wavelet transformation allows analysis of images with multiple resolution levels, providing the advantage of multi-resolution analysis [25]. Due to these capabilities, it's an effective method for extracting discriminative features from MRI images. In this study, the Discrete Wavelet Transform method was used to extract 8 features: minimum value, maximum value, mean value, standard deviation, variance, kurtosis, skewness, and entropy. These features were identified as distinctive structures in the images.

2.3.5 Histogram of Oriented Gradients(HOG) Based Features

The Histogram of Oriented Gradients (HOG) method is a powerful feature extraction technique that can characterize object information through the local density gradients of the final clustered image. HOG divides the image into different blocks, each containing a few pixels. From these pixels, the HOG feature vector is obtained. It is known that extracting too many features can be complex and unnecessary, while extracting too few features can lead to a loss of information. The HOG method, capable of characterizing object information through the local density gradients of the final clustered image, divides the image into different blocks, each containing a few pixels, from which the HOG feature vector is derived. Extracting too many features can be complex and unnecessary, while too few features can result in information loss. HOG features are extracted using various block sizes, with the best-performing size determined by testing different block sizes in the study. In this study, features were extracted using an 8 x 8 block size [26]. The feature extraction process was conducted by calculating the basic statistical characteristics of an average of 1500 features, which were used as the Histogram of Oriented Gradients feature. These features include calculations of minimum value, maximum value, mean, standard deviation, variance, skewness, kurtosis, and entropy.

2.3.6 Percentile Features

Percentile values can be utilized in feature extraction to analyze each feature based on the statistical information of the image data. Percentile values over images provide statistical information based on image pixels and the percentage associated with the image. In this study, two features representing the 10th and 90th percentiles were extracted according to the intensities of the image pixels.

As a result, a total of 48 features were calculated across all tumor types and imaging sequences in this study. Those features that were significant in distinguishing and classifying tumors were determined by applying Student's t-Test.

2.4 Machine Learning Algorithms

In our study, five different machine learning methods were used to classify the image features of tumor regions. In this study, classification processes were conducted using the Matlab program, and the results were compared. In this section, algorithms were selected considering

the data type and size, the complexity of the model, training duration, prediction performance, the interpretability and understandability of the model, and also its ability to generalize well without being prone to overfitting.

2.4.1 Support Vector Machines

In this study, tumors were initially classified using the Support Vector Machines (SVM) algorithm, which is one of the machine learning algorithms, based on significant numerical features obtained without feature extraction. Support Vector Machines, belonging to the supervised learning category, are a complex algorithm that provides high accuracy. They exhibit strong generalization capabilities and resilience against high-dimensional data. The selection of parameters holds great importance for their performance. Their training speed is comparatively slower than other algorithms. [27].

SVM is a favored algorithm for both classification and regression applications, although it is predominantly used for classification tasks. In classification applications, its goal is to accurately classify objects based on example data in the training dataset. It requires a decision plane to differentiate between different classes of data. It employs complex mathematical functions for object classification, referred to as kernels [28]. SVM has numerous advantages in applications. These advantages include high-accuracy classification in data, the ability to model complex decision boundaries, and the capability to work with datasets containing many independent variables.

In this study, six different SVM algorithms were utilized. These are as follows: Linear SVM, Quadratic SVM, Cubic SVM, Fine Gaussian SVM, Medium Gaussian SVM, Coarse Gaussian SVM.

2.4.2 Decision Trees

Decision trees typically have a flowchart-like structure where each internal node, also known as a split, represents a logical test, and each leaf represents a prediction. At each stage, each observation starts from the root and ends up in one of the leaves by following a completely transparent path. Its simplicity stems from its robustness. It is a model that is easy to understand and interpret. Decision trees can handle missing values in data, are not computationally expensive, and can make data usable in complex datasets [29].

In this study, three different decision trees were used. These are: Fine Tree, Medium Tree, Coarse Tree.

2.4.3 Logistic Regression Classifiers

Logistic regression is a powerful modeling tool and a generalization of linear regression. Logistic regression is an algorithm used to determine the shape of the relationship between dependent and independent variables for the purpose of prediction and classification. It is employed when the dependent variable has two levels. Linear regression, on the other hand, requires the dependent variable to be continuous. However, in practice, the dependent variable is often categorical and binary [30].

2.4.4 Nearest Neighbor Classifiers

The most important goal in classification is to determine, in the simplest and easiest way, to which class objects belong based on their characteristics. This algorithm is one of the simplest machine learning algorithms. It does not create an explicit prediction-based model, and data points are straightforwardly stored during training. This algorithm can be seen as a form of basic learning. In predicting a new point, the k points in the training dataset that are closest to this point in terms of distance are considered and used. When determining the nearest

neighbor, Euclidean and Manhattan distances are commonly employed. While k is a constant, it can be determined by the user [31].

In this study, 6 different KNN classifiers were used. These are: Fine KNN, Medium KNN, Coarse KNN, Cubic KNN, Cosine KNN, Weighted KNN.

2.4.5 Ensemble Classifiers

The machine learning algorithm that combines multiple models to achieve higher accuracy than a single model and reduce false positives is called an ensemble classifier [32]. This algorithm performs community-based classification by combining the prediction results of each model. This way, it ensures that the final result is obtained more accurately by learning from the errors of each individual model [33].

In this study, 5 different ensemble classifiers were used. These are: Boosted Trees, Bagged Trees, Subspace Discriminant, Subspace KNN, RUSBoost Trees.

3.Results

3.1 Feature Extraction and Results

In the study, a total of 48 features were extracted from all the images of the T1, T2, and ADC sequences, corresponding to all sections containing tumors. Significant features specific to each tumor type and image sequence were identified. Significant numerical features for all tumor types and imaging sequences were determined using the Student's t-test. In the T2 sequence, 11 significant features were found between PA and MB, while 21 significant features were identified between PA and EM, and 6 significant features between MB and EM. In the case of the ADC sequence, 28 significant features were observed between PA and MB, 6 significant features between PA and EM, and 18 significant features were found between EM and MB. Additionally, within the T1 sequence, 6 significant features were found between PA and MB, 2 significant features between EM and MB, and 2 significant features between EM and PA. Table 2, Table 3, and Table 4 below present the significant numerical features among tumor types for the T2, contrast-enhanced T1, and ADC sequences, respectively.

Table 3 Significant features obtained with posterior fossa tumor types for contrast-enhanced T1 sequence

Meaningful Features	**EM-PA**	**MB-PA**	**EM-MB**
GLCM	----------	----------	---------
DWT	Kurtosis, Skewness	Kurtosis, Skewness	---------
Primary Statistical	----------	Kurtosis, Skewness	---------
Percent Value	----------	10 Percent, 90 Percent	10 Percent, 90 Percent

Only a few of the examined features for the T1 sequence were found to be significant. Percentage value features were not significant in the T2 and ADC sequences, while they were defined as significant features for MB-PA and EM-MB tumors in the T1 sequence. Primary statistical features such as kurtosis and skewness, obtained through discrete wavelet

transform, were found to be significant among groups. This situation may be attributed to the high anatomical accuracy but limited information on tissue physiology and characteristics provided by T1 images.

Table 4 Significant features obtained between posterior fossa tumor types for the T2 sequence

Meaningful Features	**MB-PA**	**EM-PA**	**MB-EM**
GLCM	Autocorrelation, Cluster Prominence, Sum of Squares, Sum Variance	Autocorrelation,Cluster Prominence, Sum of Squares, Sum Variance,Sum Average, Information Measure of Correlation 1, Information Measure of Correlation 2	---------- -
DWT	Standart Deviation, Variance, Skewness, Entropi	Maximum Value, Mean Value,Standart Deviation, Variance, Kurtosis, Skewness	---------- -
Primary Statistical	Standart Deviation, Variance, Kurtosis	Standart Deviation, Variance	---------- -
HOG	----------	Maximum Value, Mean Value,Standart Deviation, Variance, Kurtosis, Skewness	Minimum Value, Maximum Value, Mean Value,Standart Deviation, Variance, Skewness

More distinguishing features among different tumor types in the T2 sequence were obtained compared to T1. In the ADC sequence, a greater number of significant features were obtained among all tumor types compared to the other sequences. Similar to the T2 sequence, percentage value features were not found to be significant attributes within the ADC sequence. These findings indicate that T2 and ADC sequences provide more significant features in determining the types of posterior fossa tumors. A greater number of distinguishing features between different tumor types on T2 sequence were obtained. More significant features were obtained in the ADC sequence compared to other sequences across all tumor types. Similar to the T2 sequence, percentage value features were not found to be significant features in the ADC sequence. These cases show that T2 and ADC sequences provide more meaningful features in determining the types of posterior fossa tumors.

Table 5 Significant features obtained with posterior fossa tumor types for ADC sequence

Meaningful Features	MB-PA	EM-PA	MB-EM
GLCM	Autocorrelation, Correlation 1, Correlation 2, Cluster Shade ,Cluster Prominence, Energy, Entropy, Homogeneity 1, Homogeneity 2, Maximum Probability, Sum of Squares, Sum of Squares, Sum Variance, Difference Entropy	----------	Autocorrelation, Correlation 2, Sum of Squares, Cluster Shade , Sum Average, Sum Variance
DWT	Mean Value, Standart Deviation, Kurtosis, Variance	----------	Autocorrelation, Correlation 2, Sum of Squares, Cluster Shade, Sum Average, Sum Variance
Primary Statistical	Mean Value, Standart Deviation, Kurtosis, Variance	----------	Minimum Value, Maximum Value, Standart Deviation, Variance, Kurtosis, Skewness
HOG	Maximum Value, Mean Value,Standart Deviation, Variance, Kurtosis, Skewness	Maximum Value, Mean Value,Standart Deviation, Variance, Kurtosis, Skewness	----------

3.2 Machine Learning Algorithm and Results

3.2.1 Classification results of posterior fossa tumors for T2 sequence

Different machine learning algorithms were applied to the features calculated for each type of posterior fossa tumors obtained in T1, T2 and ADC sequences. The ones that give the most successful results among these algorithms (and algorithm subtypes) are presented in the tables. For the T2 sequence, a classification process was conducted on a total of 28 individuals with posterior fossa tumors, including 5 pilocytic astrocytomas, 12 ependymomas, and 11 medulloblastomas. The classification of PA and EM tumors with decision trees is illustrated in Figure 4 below.

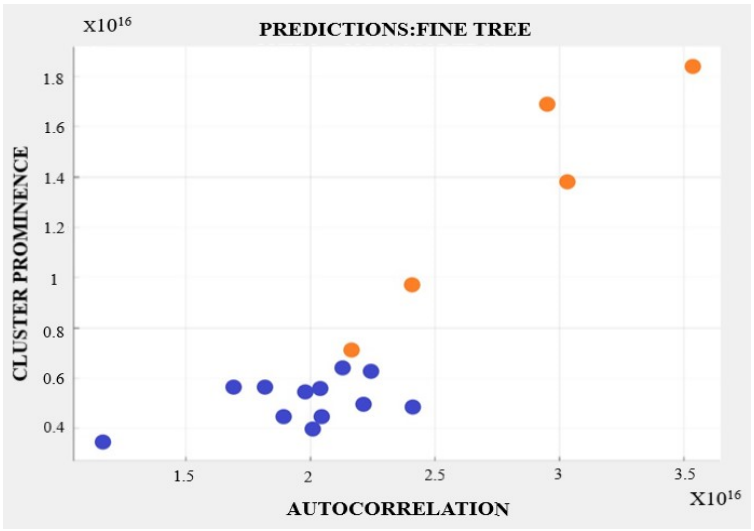

Fig. 4. The classification of PA and EM tumors captured with the T2 sequence using decision trees.

Below, the classification accuracy results obtained with five different machine learning algorithms in the T2 sequence are provided.

Table 6 The accuracy, precision, recall, and F1 score values of the classification results obtained with five different machine learning algorithms in the T2 sequence.

TUMORS	DECISION TREES	LOGISTIC REGRESSION CLASSIFIERS	SUPPORT VECTOR MACHINES	NEAREST NEIGHBOR CLASSIFIERS	ENSEMBLE CLASSIFIERS
PA-EM	94.1(%) (Fine Tree) Precision:1, Recall:0.92, F1 Score: 0.96	88.2(%) (Logistic Regression) Precision:0.916 Recall: 0.916 F1 Score: 0.916	88.2(%) (Linear SVM) Precision:1 Recall: 0.857 F1 Score: 0.924	88.2(%) (Fine KNN) Precision:1 Recall: 0.857 F1 Score: 0.924	94.1(%) (Subspace KNN) Precision:1 Recall:0.92 F1 Score: 0.96
PA-MB	100(%) (Fine Tree) Precision:1 Recall:1 F1 Score: 1	100(%) (Logistic Regression) Precision:1 Recall:1 F1 Score: 1	100(%) (Cubic SVM) Precision:1 Recall:1 F1 Score: 1	100(%) (Fine KNN) Precision:1 Recall:1 F1 Score: 1	100(%) (Subspace KNN) Precision:1 Recall:1 F1 Score: 1
EM-MB	87(%) (Fine Tree) Precision:0.818 Recall:0.9 F1 Score: 0.857	56.6(%) (Logistic Regression) Precision:0.636 Recall:0.538 F1 Score: 0.582	65.2(%) (Cubic SVM) Precision:0.545 Recall:0.666 F1 Score:0.599	78.3(%) (Fine KNN) Precision:0.454 Recall:0.555 F1 Score:0.499	69.6(%) (Bagged Trees) Precision:0.545 Recall:0.75 F1 Score:0.63

As seen in the table, the lowest successful classification occurred between EM-MB, while the highest successful classification was between PA-MB. Among the methods, decision trees provided the most successful results among the types. The ability of decision trees to directly process both numerical and categorical data, control complex models, quickly train and make

predictions on datasets, and facilitate the identification of the most influential features in determining the outcome has provided advantages in the results obtained.

3.2.2 Classification results of posterior fossa tumors for T1 sequence

For the contrast-enhanced T1 sequence, classification was performed on a total of 22 individuals with posterior fossa tumors, including 5 pilocytic astrocytomas, 7 ependymomas, and 10 medulloblastomas. The ROC curve obtained from the classification of PA and MB tumors in the contrast-enhanced T1 sequence using cubic SVM is shown in Figure 5.

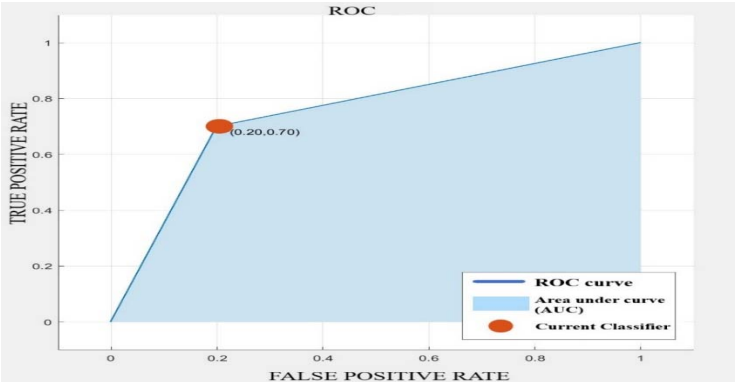

Fig. 5. The ROC curve obtained from the classification of PA and MB tumors in the T1 sequence using cubic SVM.

Below, the classification accuracy results obtained with five different machine learning algorithms in the contrast-enhanced T1 sequence are provided.

Table 7 The accuracy, precision, recall, and F1 score values of the classification results obtained with five different machine learning algorithms in the T1 sequence.

TUMORS	DECISION TREES	LOGISTIC REGRESSION CLASSIFIERS	SUPPORT VECTOR MACHINES	NEAREST NEIGHBOR CLASSIFIERS	ENSEMBLE CLASSIFIERS
PA-MB	80(%) (Fine Tree) Precision:0.8 Recall: 0.888 F1 Score: 0.842	80(%) (Logistic Regression) Precision:0.8 Recall: 0.888 F1 Score:0.842	100(%) (Quadratic SVM) Precision:1 Recall:1 F1 Score: 1	100(%) (Fine KNN) Precision:1 Recall:1 F1 Score: 1	100(%) (Bagged Trees) Precision:1 Recall:1 F1 Score: 1
PA-EM	58.3(%) (Fine Tree) Precision:0.714 Recall: 0.625 F1 Score:0.666	58.3(%) (Logistic Regression) Precision:0.714 Recall: 0.625 F1 Score:0.666	66.7(%) (Linear SVM) Precision:0.714 Recall: 0.714 F1 Score:0.714	66.7(%) (Weighted KNN) Precision:0.714 Recall: 0.714 F1 Score:0.714	66.7(%) (Subspace Discriminant) Precision:0.714 Recall: 0.714 F1 Score:0.714
EM-MB	94.1(%) (Fine Tree) Precision:1 Recall: 0.875 F1 Score:0.933	94.1(%) (Logistic Regression) Precision:1 Recall: 0.875 F1 Score:0.933	94.1(%) (Cubic SVM) Precision:1 Recall: 0.875 F1 Score:0.933	88.2(%) (Fine KNN) Precision:0.857 Recall: 0.857 F1 Score:0.857	88.2(%) (Bagged Trees) Precision:0.857 Recall: 0.857 F1 Score:0.857

As seen in the table, the lowest successful classification occurred between EM-PA, while the highest successful classification was between PA-MB. Among the methods, support vector machines provided the most successful results among the types.

3.2.3 Classification Results of Posterior Fossa Tumors for the ADC Sequence

A total of 24 individuals with posterior fossa tumors were included in the classification process for the ADC sequence, consisting of 5 pilocytic astrocytomas, 10 ependymomas, and 9 medulloblastomas.

The confusion matrix obtained from the classification of EM and MB tumors using cubic SVM is shown in Figure 6 below.

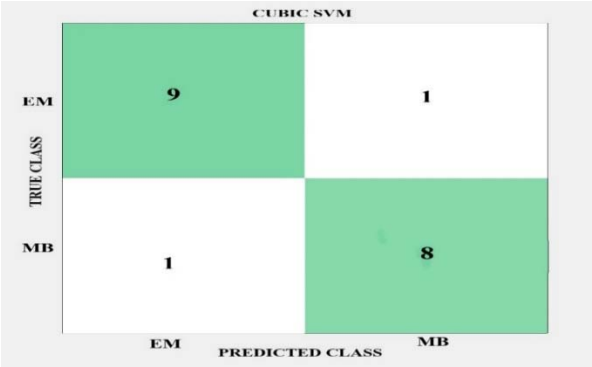

Fig. 6. The Confusion matrix obtained from the classification of EM and MB tumors in the ADC sequence using cubic SVM.

Below, the classification accuracy results obtained with five different machine learning algorithms in the ADC sequence are provided.

Table 8 The accuracy, precision, recall, and F1 score values of the classification results obtained with five different machine learning algorithms in the ADC sequence.

TUMORS	DECISION TREES	LOGISTIC REGRESSION CLASSIFIERS	SUPPORT VECTOR MACHINES	NEAREST NEIGHBOR CLASSIFIERS	ENSEMBLE CLASSIFIERS
PA-MB	71.4(%) (Fine Tree) Precision:0.777 Recall: 0.777 F1 Score:0.777	92.9(%) (Logistic Regression) Precision:0.888 Recall: 1 F1 Score:0.940	100(%) (Quadratic SVM) Precision:1 Recall:1 F1 Score: 1	85.7(%) (Fine KNN) Precision:1 Recall: 0.818 F1 Score:0.899	92.9(%) (Subspace Discriminant) Precision:0.888 Recall: 1 F1 Score:0.940
PA-EM	86.7(%) (Fine Tree) Precision:1 Recall: 0.588 F1 Score:0.741	53.3(%) (Logistic Regression) Precision:0.6 Recall: 0.666 F1 Score:0.631	86.7(%) (Linear SVM) Precision:1 Recall: 0.588 F1 Score:0.741	86.7(%) (Weighted KNN) Precision:1 Recall: 0.588 F1 Score:0.741	86.7(%) (Subspace Discriminant) Precision:1 Recall: 0.588 F1 Score:0.741
EM-MB	73.7(%) (Fine Tree) Precision:0.8 Recall: 0.727 F1 Score:0.762	78.9(%) (Logistic Regression) Precision:0.8 Recall: 0.8 F1 Score:0.8	89.5(%) (Cubic SVM) Precision:0.9 Recall: 0.9 F1 Score:0.9	84.2(%) (Medium KNN) Precision:1 Recall: 0.769 F1 Score:0.869	89.5(%) (Subspace Discriminant) Precision:0.9 Recall: 0.9 F1 Score:0.9

Our study has important implications for distinguishing between sequence types and tumor types based on the features extracted from images in three different types of posterior fossa tumors. As can be seen from the classification results presented above, all tumors were generally classified with high accuracy. In the T2 sequence, PA-MB and PA-EM tumors were classified with the highest success, while EM-MB had the lowest successful classification. With T1 sequence images, PA-EM had the lowest classification performance, PA-MB had the highest, and EM-MB had high classification accuracy. In the ADC sequence, the results were closer to each other, with the highest classification between PA-MB.

4.Discussion

Posterior fossa tumors are the most common brain tumors in childhood comprising 50–74% of pediatric all brain tumors. Majority of them are juvenile pilocytic astrocytomas, medulloblastomas, ependymomas [2, 9, 34]. Since the rapid progression of some pediatric brain tumors causes morbidity and mortality, early diagnosis of tumor types is essential. Conventional MRI has an indispensable role in the detection of brain tumors, evaluating tumor location and impact on surrounding structures, Nevertheless, it has a limited role in the diagnosis of the tumor type because pediatric posterior fossa tumors share similar appearances [35,36]. Some progress has been made to improve the diagnostic accuracy of MRI using apparent diffusion coefficient (ADC) maps, MR spectroscopy, and MR perfusion. However, these advanced MR imaging modalities did not provide accurate enough results to exactly discriminate the pediatric posterior fossa tumor types. Histopathological diagnosis is the gold standard method for the diagnosis. However, this method is time-consuming and invasive. Also, a trained neuropathologist is needed to evaluate the specimens [37, 38].

MRI-based machine learning algorithms are recently becoming an effective implement that can potentially speed up the diagnostic process. It has already been tested in the diagnosis of brain tumors in both adults and children, in differentiation of meningiomas, gliomas and pituitary tumors[39-41]. The application of MRI-based machine learning algorithms in the diagnosis of pediatric fossa tumors may improve the clinical approach for pediatric posterior fossa tumors in some potential ways. MR imaging–based classification may act as a noninvasive method to plan a surgical approach and extent of resection. Also, it may quicken the planning of any potential neoadjuvant chemotherapy, besides that the recognized imaging findings may complement the histopathology in the case of pediatric fossa tumors with complex histopathologic findings, rather than replacing the histopathologic diagnosis [10,42].

The aim of this study is to extract and classify image features that will assist radiologists in distinguishing the three most common types of posterior fossa tumors (pilocytic astrocytoma, medulloblastoma, and ependymoma) using MR images of contrast-enhanced T1, T2, and ADC sequences. The primary motivation for this research is the high mortality rate of posterior fossa tumors in children, which is attributed to the diagnostic challenges faced by radiologists in clinical settings. There are some studies in the existing literature with similar objectives and images. The study by Gutierrez et al. [10], which is the closest to our work, involved 40 children and calculated shape, histogram, and texture features from T2 and T1, as well as diffusion (ADC) sequences for EM, PA, and MB tumor types. They achieved high accuracy in classifying medulloblastomas by examining tissue features in the ADC sequence from the gray level co-occurrence matrix. The classification was performed using support vector machines, achieving a 91.4% success rate with ADC histogram features of posterior fossa tumors. Li et al.'s study [11] focused on obtaining biomarkers from machine learning-based magnetic resonance images for two different pediatric posterior fossa tumors (EM, MB) in 174 patients. They used three different feature extraction methods for 300 biomarkers and included 11 different classifiers, such as K-nearest neighbors, SVM, random forests, decision trees, neural networks, and others. The SVM classifier outperformed others, achieving 85.38% accuracy. The main differences that set our study apart from these are the use of three different imaging sequences together in the clinical diagnosis of the most common types of posterior fossa tumors and

examining all slices where the tumor is visible (an average of 5-6 sections per person), not just a single cross-sectional image. Our study also identifies which features are more distinctive in differentiating tumors from each other in each sequence's images and which machine learning algorithm provides more accurate classification using these features. These differences give our research an advantage over other studies. For all sequences, PA-MB tumors were classified with the highest accuracy. In the T2 sequence, PA-MB tumors yielded high results with all machine learning algorithms. Overall results possess high accuracy, precision, sensitivity, and F1 scores.

The most significant limitation of our study is the small sample size, due to the limited number of patients diagnosed with posterior fossa tumors in hospital records and the lack of complete image data from all three sequences for all patients with posterior fossa tumors, thus limiting the number of individuals. Therefore, future studies with more patients are expected to enhance the discriminative power of our findings. Larger datasets, supported by further studies using a broader set of features, are needed to provide more comprehensive and discriminative results and contribute to the diagnosis and treatment of posterior fossa tumors. Our study indicates the need for different feature extraction algorithms and more research in this area, as we observed few meaningful numerical features for certain imaging sequences or tumor groups during the feature extraction phase. Additionally, not limiting the classification phase to 5 methods and trying more machine learning methods could be beneficial for achieving the highest accuracy and precision in general interpretation. Moreover, using deep learning to directly classify images, apart from machine learning algorithms, could be explored. The results of our study guide future research and have the potential to support the literature and the radiology clinic.

5.Conclusions

The primary aim of this study was to differentiate childhood brain tumors, specifically pilocytic astrocytoma, medulloblastoma, and ependymoma, within posterior fossa tumor types using MR images with three different sequences. To achieve this goal, each tumor region underwent segmentation with two different image processing algorithms, confirmed by a radiologist. Subsequently, numerical feature extraction was performed using five different methods from the segmented images. This ensured the extraction of 48 different numerical features for each tumor, and significant numerical features were identified for each sequence and tumor type. During the feature extraction stage, a limited number of significant features were identified for some tumor groups. Among the imaging sequences, the ADC sequence provided the most significant features, while the contrast-enhanced T1 sequence yielded fewer significant numerical features. Subsequently, classification was performed for each sequence and tumor type using five different machine learning methods. When considering all sequences together, the highest success for PA-EM was achieved with 100% accuracy from the T2 sequence, for PA-MB with 100% accuracy from the T2 and contrast-enhanced T1 sequences, and for EM-MB with 89.5% accuracy from the ADC sequence. The results of our study hold promise for the classification of posterior fossa tumors in future research. Increasing the sample size, utilizing more comprehensive feature extraction methods to increase the number of significant features, and experimenting with various machine learning algorithms can further enhance classification results.

Conflicts of Interest

The author has no conflicts of interest to declare.

References

1. Lannering B, Marky I, & Nordborg, C. (1990). Brain tumors in childhood and adolescence in west sweden 1970–1984 epidemiology and survival. Cancer, 66(3), 604-609.
2. Prasad, K. S. V., Ravi, D., Pallikonda, V., & Raman, B. V. S. (2017). Clinicopathological study of pediatric posterior fossa tumors. Journal of pediatric neurosciences, 12(3), 245.
3. KaatschP, RickertC,KühlJ, Schüz J, Michaelis J. Population-based epidemiologic data on brain tumors in German children. Cancer 2001;92(12):3155–64
4. O'Brien D, Caird J, Kennedy M, et al. Posterior fossa tumours in childhood: evaluation of presenting clinical features. Ir Med J 2001;94:52–53
5. Orphanidou-Vlachou, E., Vlachos, N., Davies, N.P., Arvanitis, T.N., Grundy, R.G., and Peet, A.C., 2014. Texture analysis of T1-and T2-weighted MR images and use of probabilistic neural network to discriminate posterior fossa tumours in children, NMR in Biomedicine, 27(6):632–639.
6. Zhou, H., Hu, R., Tang, O., Hu, C., Tang, L., Chang, K., ... & Zhu, C. (2020). Automatic machine learning to differentiate pediatric posterior fossa tumors on routine MR imaging. American Journal of Neuroradiology, 41(7), 1279-1285.
7. Traverso A, Wee L, Dekker A, Gillies R. Repeatability and reproducibility of radiomic features: a systematic review. Int J Radiat Oncol Biol Phys 2018;102(4):1143–58
8. Wang, S., Wang, G., Zhang, W., He, J., Sun, W., Yang, M., ... & Peet, A. (2022). MRI-based whole-tumor radiomics to classify the types of pediatric posterior fossa brain tumor. Neurochirurgie, 68(6), 601-607.
9. Bidiwala, S., & Pittman, T. (2004). Neural network classification of pediatric posterior fossa tumors using clinical and imaging data. Pediatric neurosurgery, 40(1), 8-15.
10. Gutierrez, D. R., Awwad, A., Meijer, L., Manita, M., Jaspan, T., Dineen, R. A., ... & Auer, D. P. (2014). Metrics and textural features of MRI diffusion to improve classification of pediatric posterior fossa tumors. American Journal of Neuroradiology, 35(5), 1009-1015.
11. Li, M., Shang, Z., Yang, Z., Zhang, Y., & Wan, H. (2019). Machine learning methods for MRI biomarkers analysis of pediatric posterior fossa tumors. Biocybernetics and Biomedical Engineering, 39(3), 765-774.
12. Zarinabad, N., Abernethy, L. J., Avula, S., Davies, N. P., Rodriguez Gutierrez, D., Jaspan, T., ... & Peet, A. (2018). Application of pattern recognition techniques for classification of pediatric brain tumors by in vivo 3T 1H-MR spectroscopy—A multi-center study. Magnetic Resonance in Medicine, 79(4), 2359-2366.
13. Sotoudeh, H., Saadatpour, Z., Rezaei, A., Sotoudeh, M., Wheeler, C.A., Singhal, A., and Tanwar, M., 2023. Radiomics for differentiation of the posterior fossa pilocytic astrocytoma versus hemangioblastomas in adults. A pilot study, Clinical Imaging, 93:26–30.
14. Li, M., Wang, H., Shang, Z., Yang, Z., Zhang, Y., and Wan, H., 2020. Ependymoma and pilocytic astrocytoma: Differentiation using radiomics approach based on machine learning, Journal of Clinical Neuroscience, 78:175–180.
15. Quon, J., Bala, W., Chen, L., Wright, J., Kim, L., Han, M., Shpanskaya, K., Lee, E., Tong, E., Iv, M., et al., 2020. Deep learning for pediatric posterior fossa tumor detection and classification: a multi-institutional study, American Journal of Neuroradiology, 41(9):1718–1725.
16. Fetit, A.E., Novak, J., Rodriguez, D., Auer, D.P., Clark, C.A., Grundy, R.G., Peet, A.C., and Arvanitis, T.N., 2018. Radiomics in paediatric neuro-oncology: a multicentre study on MRI texture analysis, NMR in Biomedicine, 31(1):e3781.
17. Osmanoğlu, Usame Ömer, et al. "Görüntü işleme ve analizinin tıpta kullanımı ve bir uygulama." Osmangazi Tıp Dergisi 41.1 (2016): 6-16.

18. Borman, S. (2004). The expectation maximization algorithm-a short tutorial. Submitted for publication, 41.
19. Lankton, S., & Tannenbaum, A. (2008). Localizing region-based active contours. IEEE transactions on image processing, 17(11), 2029-2039.
20. Bozkurt, Ferhat, Cemal Köse, and Ahmet Sarı. "Bolge-tabanlı Aktif Kontur ve Sınıflandırma ile BTA Goruntulerinden Karotid Arterlerin Bolutlenmesi."
21. Chan, T. F., & Vese, L. A. (2001). Active contours without edges. IEEE Transactions on image processing, 10(2), 266-277.
22. Zulpe, N., & Pawar, V. (2012). GLCM textural features for brain tumor classification. International Journal of Computer Science Issues (IJCSI), 9(3), 354.
23. Saman, S., & Jamjala Narayanan, S. (2019). Survey on brain tumor segmentation and feature extraction of MR images. International journal of multimedia information retrieval, 8, 79-99.
24. Chaudhary, A., & Bhattacharjee, V. (2020). An efficient method for brain tumor detection and categorization using MRI images by K-means clustering & DWT. International Journal of Information Technology, 12, 141-148.
25. Faisal, Z., & El Abbadi, N. K. (2020). Detection and recognition of brain tumor based on DWT, PCA and ANN. Indonesian Journal of Electrical Engineering and Computer Science, 18(1), 56-63.
26. Mostafiz, R., Uddin, M. S., Alam, N. A., Hasan, M. M., & Rahman, M. M. (2021). MRI-based brain tumor detection using the fusion of histogram oriented gradients and neural features. Evolutionary Intelligence, 14, 1075-1087.
27. Singh, A., Thakur, N., & Sharma, A. (2016, March). A review of supervised machine learning algorithms. In 2016 3rd international conference on computing for sustainable global development (INDIACom) (pp. 1310-1315). Ieee.
28. Ray, S. (2019, February). A quick review of machine learning algorithms. In 2019 International conference on machine learning, big data, cloud and parallel computing (COMITCon) (pp. 35-39). IEEE.
29. Costa, V. G., & Pedreira, C. E. (2023). Recent advances in decision trees: An updated survey. Artificial Intelligence Review, 56(5), 4765-4800.
30. ÇİÇEK, A., & ARSLAN, Y. (2020). Müşteri Kayıp Analizi İçin Sınıflandırma Algoritmalarının Karşılaştırılması. İleri Mühendislik Çalışmaları ve Teknolojileri Dergisi, 1(1), 13-19.
31. De Lucia, C., Pazienza, P., & Bartlett, M. (2020). Does good ESG lead to better financial performances by firms? Machine learning and logistic regression models of public enterprises in Europe. Sustainability, 12(13), 5317.
32. Zhou, Y., Cheng, G., Jiang, S., & Dai, M. (2020). Building an efficient intrusion detection system based on feature selection and ensemble classifier. Computer networks, 174, 107247.
33. Guo, Z., Xu, L., & Ali Asgharzadeholiaee, N. (2022). A homogeneous ensemble classifier for breast cancer detection using parameters tuning of MLP neural network. Applied Artificial Intelligence, 36(1), 2031820.
34. O'Brien D, Caird J, Kennedy M, et al. Posterior fossa tumours in childhood: evaluation of presenting clinical features. Ir Med J 2001;94:52–53
35. Brandão, L. A., & Poussaint, T. Y. (2017). Posterior fossa tumors. Neuroimaging Clinics, 27(1), 1-37.
36. Kerleroux B, Cottier JP, Janot K, et al. Posterior fossa tumors in children: radiological tips & tricks in the age of genomic tumor classification and advance MR technology. J Neuroradiol 2020;47:46–53
37. Jaremko, J. L., Jans, L. B. O., Coleman, L. T., & Ditchfield, M. R. (2010). Value and limitations of diffusion-weighted imaging in grading and diagnosis of pediatric posterior fossa tumors. American journal of neuroradiology, 31(9), 1613-1616.
38. Schneider, J. F., Confort-Gouny, S., Viola, A., Le Fur, Y., Viout, P., Bennathan, M., ... & Girard, N. (2007). Multiparametric differentiation of posterior fossa tumors in

children using diffusion-weighted imaging and short echo-time 1H-MR spectroscopy. Journal of Magnetic Resonance Imaging: An Official Journal of the International Society for Magnetic Resonance in Medicine, 26(6), 1390-1398.
39. Pringle, C., Kilday, J. P., Kamaly-Asl, I., & Stivaros, S. M. (2022). The role of artificial intelligence in paediatric neuroradiology. Pediatric Radiology, 52(11), 2159-2172.
40. Ismael, S. A. A., Mohammed, A., & Hefny, H. (2020). An enhanced deep learning approach for brain cancer MRI images classification using residual networks. Artificial intelligence in medicine, 102, 101779.
41. Buchlak, Q. D., Esmaili, N., Leveque, J. C., Bennett, C., Farrokhi, F., & Piccardi, M. (2021). Machine learning applications to neuroimaging for glioma detection and classification: An artificial intelligence augmented systematic review. Journal of Clinical Neuroscience, 89, 177-198.
42. Massimino, M., Cefalo, G., Riva, D., Biassoni, V., Spreafico, F., Pecori, E., ... & Gandola, L. (2012). Long-term results of combined preradiation chemotherapy and age-tailored radiotherapy doses for childhood medulloblastoma. Journal of neuro-oncology, 108, 163-171.